Research Article Vol. 14, No. 8 / 1 Aug 2023 / Biomedical Optics Express 4170
Biomedical Optics EXPRESS

Application of fluorescence lifetime imaging microscopy to monitor glucose metabolism in pancreatic islets *in vivo*

ZHONGYING WANG,[1,†] MAANI ARCHANG,[1,†] TATYANA GURLO,[1] ELAINE WONG,[1] SCOTT E. FRASER,[2] AND PETER C. BUTLER[1,*]

[1]*Larry L. Hillblom Islet Research Center, University of California Los Angeles, David Geffen School of Medicine, Los Angeles, CA 90095, USA*
[2]*Department of Biological Sciences, Bridge Institute, David Dornsife College of Letters, Arts and Sciences, University of Southern California, Los Angeles, CA 90089, USA*
[†]These authors contributed equally to this work.
[*]*PButler@mednet.ucla.edu*

Abstract: Glucose stimulated insulin secretion is mediated by glucose metabolism via oxidative phosphorylation generating ATP that triggers membrane depolarization and exocytosis of insulin. In stressed beta cells, glucose metabolism is remodeled, with enhanced glycolysis uncoupled from oxidative phosphorylation, resulting in the impaired glucose-mediated insulin secretion characteristic of diabetes. Relative changes in glycolysis and oxidative phosphorylation can be monitored in living cells using the 3-component fitting approach of fluorescence lifetime imaging microscopy (FLIM). We engrafted pancreatic islets onto the iris to permit in vivo FLIM monitoring of the trajectory of glucose metabolism. The results show increased oxidative phosphorylation of islet cells (~90% beta cells) in response to hyperglycemia; in contrast red blood cells traversing the islets maintained exclusive glycolysis as expected in the absence of mitochondria.

1. Introduction

Blood glucose levels are closely regulated to ensure an adequate supply for brain function and to prevent the deleterious effects of hyperglycemia. This regulation depends largely on pancreatic beta cells that secrete insulin in response to increasing glucose concentrations. The close linkage between the circulating glucose concentrations and the rate of insulin secretion is mediated by metabolism of glucose by beta cells.

Evaluating metabolism in pancreatic beta cells has most frequently been accomplished in isolated islets under circumstances where blood flow is absent resulting in a gradient of nutrients and oxygen from the periphery to the core of the islet that is not present in life. To overcome this limitation, several groups have transplanted islets into the anterior chamber of the eye in mice, a strategy that permits direct imaging of live vascularized islets [1–3].

We previously applied the phasor approach of fluorescence lifetime imaging microscopy (FLIM) to evaluate shifts in glucose metabolism in isolated islets [4]. FLIM exploits the different fluorescence lifetimes of free NAD(P)H versus bound NAD(P)H [5]. Free NAD(P)H is generated by glycolysis and the pentose pathway whereas bound NAD(P)H is predominantly generated by oxidative phosphorylation (OxPhos). Therefore, changes in the ratio of free/bound NAD(P)H provide insights into shifts in glucose metabolism.

In the present study we extended the use of FLIM to live cell imaging of changes in islet cell metabolism in response to glucose in living vascularized pancreatic islets implanted into the anterior chamber of the mouse eye (ACE) site, which has been used as imaging site for the study of islet blood flow [6], diabetes immunopathology [7], NAD(P)H response [8], and calcium

#493722 https://doi.org/10.1364/BOE.493722
Journal © 2023 Received 16 May 2023; revised 9 Jul 2023; accepted 10 Jul 2023; published 19 Jul 2023

Biomedical Optics EXPRESS

dynamics [9]. This novel imaging approach offers a powerful tool to evaluate novel therapeutic candidates for diabetes.

2. Methods

2.1. Animals

All experiments involving animals, animal cells or tissues were performed in accordance with the Animal Research Committee (ARC) ethical guidelines at UCLA under protocol ARC#2004-119. FVB mice were originally purchased from Charles River laboratory, and the colony was maintained at UCLA. 8-10-week-old male mice were used as donors for islet isolation or recipients for islet transplants.

2.2. Islet isolation and transplantation into the anterior chamber of the eye

Mouse islets were isolated from the pancreas as previously described [10] and cultured overnight to recover. 20-50 islets with a diameter less than 250 µm were picked into a 0.3 mL PCR tube, washed once with FBS-free media, and pelleted by 2,000 x g, 3 sec. The pellet was then moved to a culture plate in a 20 µL volume using a pipette. A custom made curved 1/2" 27 G canula (400 µm O.D., 340 µm I.D.) was connected to a 0.1 mL Hamilton GasTight Syringe via a 0.5 mm ID Tygon tubing filled with FBS-free media; the syringe, mounted on a HARVARD PHD2000 syringe pump, was used for loading and transplantation of islets. Under the stereoscope, islets were loaded into the canula in less than 4 µL volume with the syringe pump set at 20 µL/min.

Recipient mice were anesthetized with 2.5% isoflurane inhalation and placed on a heating pad under a stereoscope with an inhalation mask attached. Using the tip of a disposable insulin syringe (29 - 31 G), a single lateral incision was made at the midpoint between the apex of the cornea and the limbus.

Islets were injected into the anterior chamber of the eye (ACE), and allowed to settle onto the iris, using the infuse function of the pump set at 10 µL/min in less than 4 µL volume. A drop of proparacaine hydrochloride 0.5% and antibiotic ophthalmic ointment were applied to the transplanted eye. The anesthetized mouse was kept in the same position for 10-15 minutes after the injection procedure to facilitate engraftment of the islets at the position they settled on the iris.

2.3. Induction of anesthesia and preparation of mouse for FLIM imaging

Anesthesia was induced with fluanisone-fentanyl-midazolam (FFM; 25/0.63/12.5 mg/kg), injected intraperitoneally [11]. Mice were then intubated with a 1" 20 G I.V. catheter connected to a MiniVent 845 ventilator (Hugo Sachs Elektroniks, Germany), and ventilated at 250 µL tidal volume and 150 breaths/min with room air. Anesthesia was maintained by intraperitoneal infusion of (fluanisone-fentanyl at 25/0.63 mg/kg/h) [11]. Naloxone was administered (1.2 mg/kg) to reverse the respiratory suppression that can result from FFM.

When performing brightfield imaging only, to evaluate the islet location and morphology, the mouse was anesthetized with 2.5% isoflurane and then mounted onto the head holder equipped with a gas mask, without the need for IP catheter or ventilator.

2.4. Imaging islets in the anterior chamber of the eye

The head of the anesthetized animal was immobilized with the transplanted eye positioned upward, on a customized microscope stage with a heating pad to control body temperature and stands to hold the head holder (Narishige, SGM-4) and a micromanipulator with magnetic stand (Narishige, UM-3FC, USM-10, URC-4) (Fig. S1B) adapted from Matilda Chan's protocol [12]. A metal loop held in forceps (Dumont No. 5, Fine Science Tools, 11251-10) was gently brought to the corneoscleral junction using the micromanipulator to stabilize the eye and diminish movements with breathing (Fig. S1B, C).

Biomedical Optics EXPRESS

A 25x water immersion objective (HC PL IRAPO 25x/0.75) was used for imaging on an upright Leica TCS-SP8-MP Deep In Vivo Imaging System, equipped for confocal laser scanning microscopy (LSM) and two photon laser scanning microscopy (TPLSM). Two-photon excitation was provided by an InSight X3 + tunable ultrafast laser at 80 MHz; autofluorescence emission was detected by two external FLIM HyD detectors (Leica 4Tune HyD detector). The FLIM signal was collected at 512×512 format, which provides sufficient resolution for the study of islet and vasculature architecture and cell nucleus structure. The laser was set to an average power of 0.35 mW with a scanning speed of 200 Hz using "line repeats" mode. NADH and NADPH were excited by two-photon illumination at 740 nm; autofluorescence was detected at 440-500 nm emission range.

2.5. Glucose stimulation

After baseline FLIM imaging, glucose stimulation (2 g/kg) was administered by intraperitoneal injection of a 20% dextrose solution (Phoenix Pharmaceutical, Inc.) in saline (0.2-0.3 ml). Blood glucose concentration was measured before and 30 mins after glucose injection using FreeStyle Lite blood glucometer. Blood samples were collected from mouse orbital into EDTA anticoagulant tubes before and 30 min after glucose stimulation. Plasma was removed from the cell pellet after centrifugation and plasma insulin concentration was measured using a mouse insulin ELISA kit (Mercodia, 10-1247-10).

2.6. Immunostaining and imaging

For histological analysis, the enucleated eye globe was fixed by immersion in 4% paraformaldehyde at 4°C overnight. The globe was then washed 3x in PBS, dehydrated, embedded in paraffin blocks, and sectioned at 4 μm thickness. For immunofluorescent staining, after rehydration and antigen retrieval in citrate-based buffer (pH 6.0), tissue sections were permeabilized in 0.4% TritonX-100 in TBS (Tris-buffered saline) for 30 min and blocked with 3% BSA + 0.2% Triton X-100 in TBS for 1 h. Sections were stained with primary antibodies diluted in TBS with 3%BSA + 0.2%Tween-20 overnight at 4°C, followed by a cocktail of secondary antibodies for 1 hour at room temperature. The manufacturer and the dilution used for each antibody is presented in Table S1. Three 5-minute washes were performed after each antibody incubation. Immunofluorescence stained sections were mounted in Vectashield with DAPI. For immunohistochemistry staining, tissue sections were treated with 10% methanol and 3% H_2O_2 in TBS, blocked with BSA in Tris B buffer (0.1 M Tris, 0.85% NaCl, 0.1% Triton X-100, 2% BSA, pH 7.4–7.6). After incubation with insulin antibody diluted in Tris B buffer and TBS-T washing, slides were then stained using DAB-peroxidase kit from Vector Laboratories and hematoxylin and Eosin. Slides were dehydrated and coverslipped with Permount. Slides were imaged using Zeiss Axio Imager M2.

2.7. FLIM data analysis

For the analyses reported here, the FLIM data was analyzed using the LAS X FLIM/FCS (Version 3.5.6, Leica Microsystems, Inc, Buffalo Grove, IL). Pseudo-colored Fast FLIM image was generated based on photon arrival times in each pixel without binning. For the fitting analysis, an average of 10,000 photons per decay curve were collected by aggregating all eligible pixels. The intensity gate was set to 10 to eliminate background pixels. The fitting analysis was performed using the n-Exponential Reconvolution model. χ^2, lifetime and intensity were exported and further statistical analysis was performed in Graphpad Prism (Graphpad Software, Inc, San Diego, CA). Statistical analysis of changes after glucose stimulation was undertaken by a two-tailed paired Wilcoxon test.

For the time-domain approach, a multi-component fitting model was applied. It has been widely established that the decay curve of NAD(P)H fluorescence most readily fit a biexponential decay curve that distinguishes between short lifetime of free NAD(P)H (0.3-0.8 ns) and longer

Biomedical Optics EXPRESS

lifetime of bound NAD(P)H (1-6.5 ns) [13–15]. We validated our analysis pipeline by reproducing their findings using a pancreatic beta cell line (INS823/13), and then used this validated approach in mouse islets transplanted into the anterior chamber of the eye (Fig. S2A). The decay curves of NAD(P)H fluorescence fit a biexponential curve in both the beta cell line and transplanted islets (Table S2, Fig. S2B). The χ^2 value of 2 component fitting in islets was poorer than in cell lines (Table S2, 14.4 ± 12.4), likely due to the more complex 3D anatomy of the islet tissue. Thus, we constrained the fit by taking advantage of the known lifetime of free NAD(P)H (0.4 ns) and longer lifetimes of bound NADPH [16–18] versus bound NADH to generate a better fit for the islet decay curve by decomposing the data into three component curves. To account for the effect of red blood cells with high NADPH content related to ROS production on evaluation of the islet oxidative phosphorylation, we separated the bound NADH signal from the bound NADPH signal. The $\chi 2$ of 3-component fitting of ACE islets (Table S2, 3.69 ± 2.36) was improved comparing to 2-components-fitting, but still slightly higher than 3. This can be caused by the limited photon budget and complexity of the tissue samples. Fits using more than 3 components in INS823/13 cells showed no improvement of $\chi 2$, perhaps limited by photon counts. The values of $\tau 1$, $\tau 2$ and $\tau 3$ were not altered by glucose stimulation (Fig. S2C, S2D). The intensities (I_1, I_2, I_3) of the three lifetime components ($\tau 1$, $\tau 2$, $\tau 3$) were used to delineate the contribution of free NAD(P)H ($\tau 1$, I_1), bound NADH ($\tau 2$, I_2) and bound NADPH ($\tau 3$, I_3). The oxidative phosphorylation level was evaluated as the ratio of the intensity from bound NADH (I_2) over intensity from total NAD(P)H ($I_{total} = I_1 + I_2 + I_3$): $I_2/(I_{total})$.

3. Results

3.1. Pancreatic islets implanted onto the iris for live cell imaging

To permit live cell imaging of pancreatic islets, islets were injected into the anterior chamber of the eye of the FVB strain of mice where they subsequently implanted onto the iris (Fig. 1). Islets engrafted close together on the iris tend to subsequently merge into a single large islet cluster (Fig. 1(B)). For our imaging analyses, we selected the islets that remained single, reasoning these retain a cellular architecture more closely represented of islets within the pancreas. The most abundant cell type in the transplanted islets was beta cells (Fig. 1(C)-(F)). Alpha cells were found only at the periphery of the transplanted islets, at numbers less than in mouse islets in the pancreas, presumably reflecting the preferential loss of alpha cells during islet isolation and engraftment (Fig. 1(F)).

Imaging studies were carried out four months after islet transplant to allow an adequate time for the development of a blood supply from the iris. As detailed in Methods, mice were anesthetized, intubated, and secured on a heating pad; the eye was stabilized and oriented for live islet imaging with a loop holder (Fig. S1).

3.2. Islets implanted on the iris are vascularized

At the onset of imaging, the eye was visually inspected in the brightfield mode to identify islets and the blood vessels that provided circulation to the islets. A candidate islet was selected based on the presence of intra-islet blood vessels, which was imaged using the 25x objective to observe the rapid transit of red blood cells through vessels traversing the islet (Fig. 2(A) and Visualization 1).

To image the autofluorescence generated by NAD(P)H, the islet was scanned by 2-photon laser excitation at 740 nm and the 440nm-500 nm emission range was collected to determine the fluorescence lifetimes of each pixel. The FLIM analysis was used to visualize the structure and NAD(P)H metabolic states of engrafted islets in isolated islets [4]. The NAD(P)H signal was pseudo-colored based on photon arrival times to present the average lifetime and relative proportions of free versus bound NAD(P)H in each pixel (Fig. 2(B)): blue depicts the shorter

Biomedical Optics EXPRESS

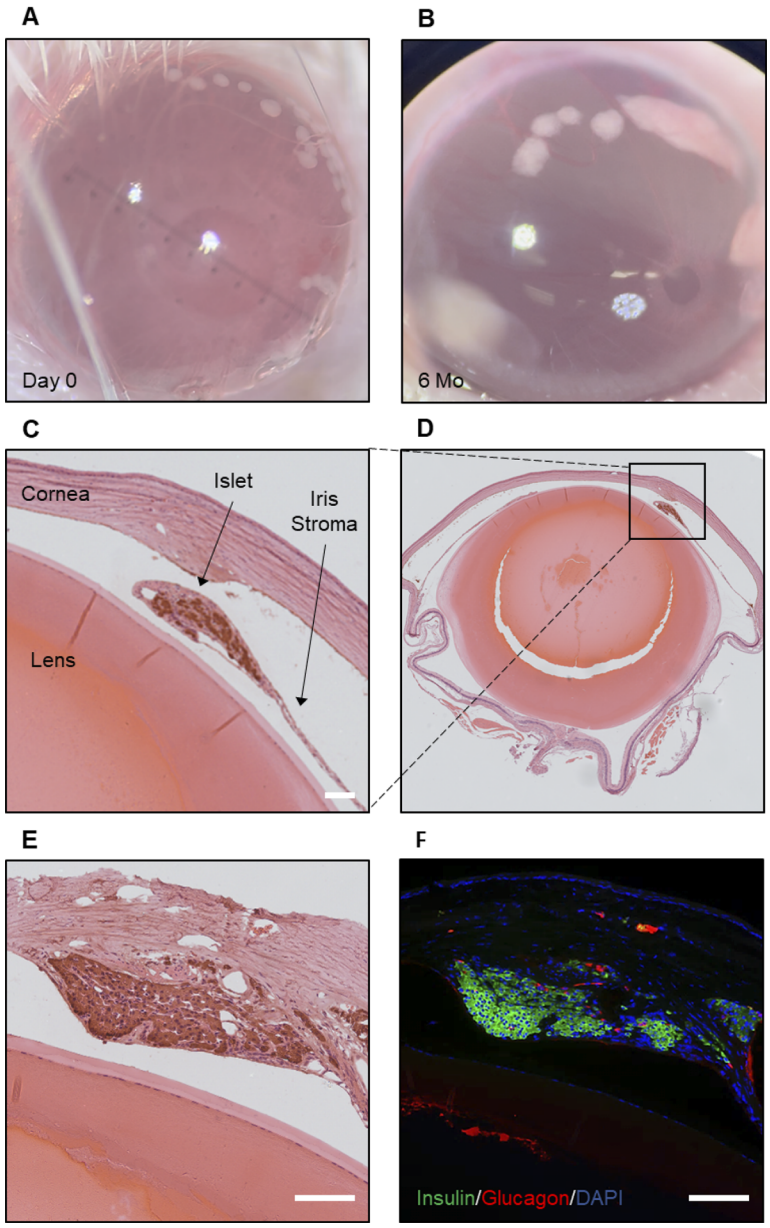

Fig. 1. SURVIVAL AND BETA CELL DOMINANCE IN ISLET TRANSPLANTED INTO THE ANTERIOR CHAMBER OF THE EYE (ACE). Mouse islets transplanted into the anterior chamber of the mouse eye (A-E) offer an accessible population of vascularized beta cells in vivo. (A, B) Representative bright field images of transplanted islets on day 0 and 6 months after transplantation. (C-E) Coronal sections through eye showing transplanted islets in the iris (immune-positive for insulin by Insulin-DAB and Hematoxylin stains). (F) To establish the relative proportions of the most abundant islet endocrine cells, we carried out Immunofluorescence staining of adjacent sections for insulin (green, beta cells) and glucagon (red, alpha cells), cell nuclei are stained with DAPI (blue). Beta cells were the most abundant cell type (more than 90%) in the transplanted islets; alpha cells were reduced in numbers compared to islets in the pancreas but primarily located at the periphery. Scale bar, 100μm.

Biomedical Optics EXPRESS

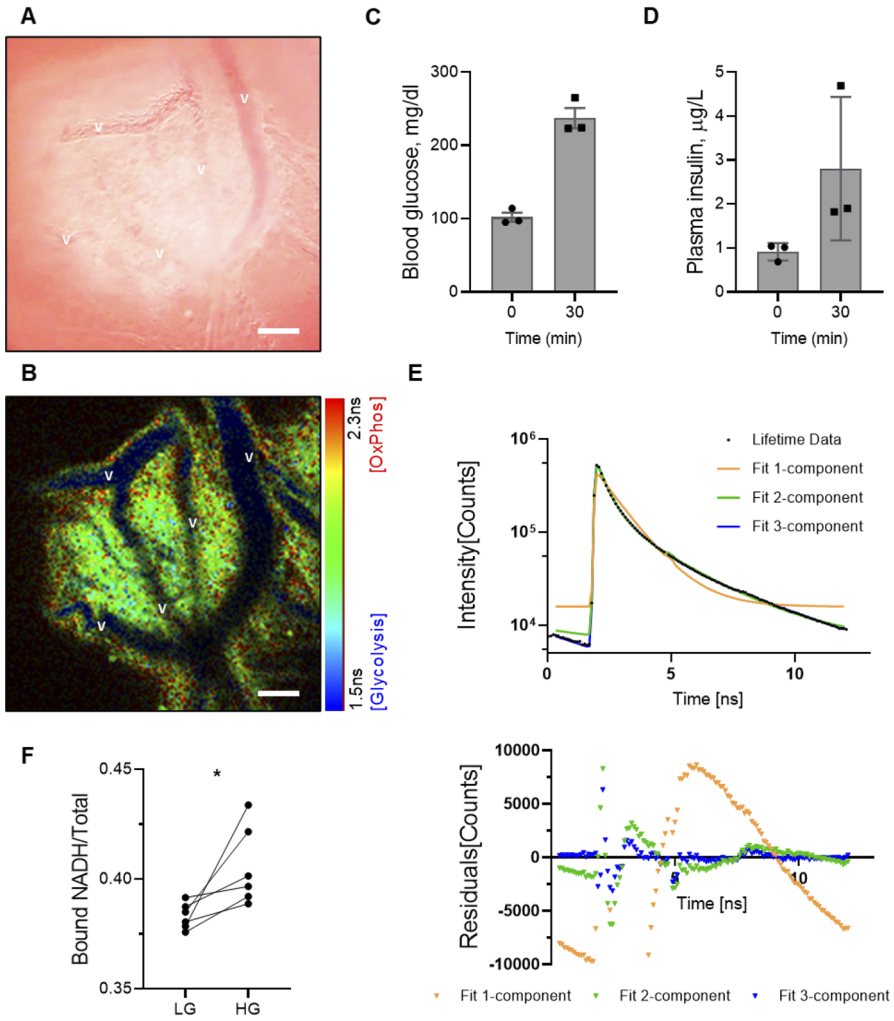

Fig. 2. FLIM ANALYSIS OF TRANSPLANTED ISLETS UNDER GLUCOSE CHALLENGE. Once the mouse is in position we first identify a candidate islet in the iris by bright field imaging (A). The islets are more reflective (brighter) than the surrounding iris with red cells visible traversing prominent blood vessels penetrate the islets (supplemental movie 1). (B) Once the candidate islet is selected, we carry out FLIM imaging and the islet image is subsequently pseudo-colored by use of average lifetime in each pixel – high ratio of shorter lifetime free NAD(P)H depicting glycolysis in blue and bound NAD(P)H predominantly representing oxidative phosphorylation in red, green and yellow revealing intermediate proportions of free and bound NAD(P)H. The lumen of the blood vessels reveals predominant free NAD(P)H (blue) consistent with the predominant glycolysis in red blood cells that have no mitochondria. The rest of the islet, shows a range of intermediate (green/yellow) to high levels (red) of oxidative phosphorylation Scale bar, 50µm. (C,D) To evaluate the islet response to hyperglycemia, FLIM imaging is performed in the same islet in the fasting state and then 30 minutes later after an intraperitoneal glucose injection that increased blood glucose (C) and plasma insulin concentrations (D). (E) Improved fitting pattern (top panel) and decreased residuals (bottom panel) were observed by fitting the representative FLIM data of islet (black dots) using 1-, 2-, or 3-component exponential decay models. (F) Computing the changes in bound NADH/total NAD(P)H based on 3-components fitting strategy, there was a consistent increase in response to hyperglycemia induced increased insulin secretion. *, $p < 0.05$, $n = 6$, two-tailed paired Wilcoxon test.

Biomedical Optics EXPRESS

lifetime free NAD(P)H generated by glycolysis; green, yellow and red represent progressively greater fractions of the longer-lived bound NAD(P)H fluorescence (predominantly oxidative phosphorylation). The FLIM image provides clear visualization of blood vessels. As anticipated, the red blood cell NAD(P)H fluorescence exhibited predominantly short lifetimes, which aligns with glycolytic metabolism.

3.3. Live cell imaging of vascularized islets, and response to glucose

Having established FLIM in the vascularized islet in vivo, we then applied this approach to monitor the transition of islet cell metabolism from the fasting state to 30 minutes after an intraperitoneal injection of glucose that increased blood glucose from 120 ± 12 to 295 ± 46 mg/dl (Fig. 2(C)). During this same period plasma insulin increased from 0.8 ± 0.2 to 3.2 ± 1.4 µg/L (Fig. 2(D)).

To evaluate oxidative phosphorylation in islets, instead of simply considering two components – free NAD(P)H and protein-bound NAD(P)H, we needed to separate the bound NADH signal from the bound NADPH signal. This separation was necessary due to the presence of other cell types, such as red blood cells, with high levels of NADPH. We processed FLIM data using a validated 3-component model to study the fluorescence lifetime parameters of protein bound-NADH (Table S2, $\tau 2 = 1.39 \pm 0.08$) and bound-NADPH ($\tau 3 = 5.32 \pm 0.37$), while setting the free-NAD(P)H lifetime to 0.4 ns ($\tau 1 = 0.4$) as previously described by Zagaynova et al. [18]. Fitting the 3 components decreased fitting residuals and improved goodness of fit ($\chi^2 = 3.69 \pm 2.36$) supporting the validity of the 3-component model for the *in vivo* study and allowed to analyze intensity contribution of each component to total NAD(P)H fluorescence (I_{total}) (Fig. 2(E), Fig. S2B). The increase in the contribution of bound NADH (Bound NADH/Total NAD(P)H = I_2/ I_{total}) in response to glucose signifies the enhancement of oxidative phosphorylation, which is consistent with the augmented insulin secretion mediated by ATP generated from oxidative phosphorylation (Fig. 2(F)). We were able successfully monitor transplanted islet activity for at least 4 months (the latest time point in our study).

4. Discussion

In health, blood glucose levels are maintained in a narrow range by the closed-loop feedback between glucose-stimulated insulin-secretion and the actions of insulin to lower blood glucose. Glucose-regulated insulin-secretion by pancreatic beta cells relies on coupling of the prevailing glucose concentration with proportionate metabolism of glucose by oxidative phosphorylation [19]. The tight metabolic coupling of the blood glucose concentration with the rate of insulin secretion is dysfunctional in diabetes [20]. Under conditions of beta cell stress, whether immune or non-immune mediated, genes that are normally disallowed in beta cells, such as lactate dehydrogenase (LDH), are expressed, uncoupling glycolysis from oxidative phosphorylation and contribute to hyperglycemia in diabetes [21,22].

Until recently, most studies of beta cell metabolism relied on measurement of the expression of relevant genes in isolated islets or pancreas sections. This approach is indirect, and since it is performed in non-living cells, it cannot be carried out more than once in the same islets. We previously applied FLIM to monitor the relative flux through glycolysis and oxidative phosphorylation in response to a glucose challenge in living isolated pancreatic islets [4]. While mechanistically informative, there are limitations in applying FLIM to isolated islets, including that are they are no longer vascularized, are subject to the perturbations introduced by recent collagenase digestion and studies cannot be repeated in the same islets over any extended time, for example to evaluate the efficacy of a novel therapy.

In the present studies we extend the application of FLIM to permit the evaluation of the metabolic trajectory in vascularized islet in vivo. By transplanting islets into the anterior chamber of the eye, the islets can obtain functional circulation from the iris in the weeks after

Biomedical Optics EXPRESS

transplantation. This site permits direct visualization of the same pancreatic islets, potentially on multiple occasions over time. As performed here, the spatial resolution of the imaging of the transplanted islets is less than was obtained in the isolated islets, which does not allow FLIM analyses of individual endocrine cells. However, the preferential loss of alpha cells results in an over-representation of beta cells (>90% in the transplanted islets), permitting metabolic analysis of the beta cell response from the aggregate analysis of the islets, showing the increased in oxidative phosphorylation expected of beta cells in response to hyperglycemia.

In our current study, we established the application of FLIM in non-diabetic male mice islets. Considering the excellent compatibility of ACE transplantation within and between species [7], it would be beneficial to investigate and compare the FLIM results of islets from both genders in the future research. Application of FLIM to vascularized islets in vivo also provides a reassuring negative control for evaluation of oxidative phosphorylation. In contrast to beta cells, red blood cells traversing the transplanted islets exhibited a FLIM signature of glycolysis, consistent with their lack of mitochondria.

5. Conclusion

In the present studies we have established the application of FLIM to monitor the relative trajectory of glycolysis and oxidative phosphorylation in vascularized living pancreatic islets in response to glucose stimulation. This approach opens the possibility to evaluate the impact of novel medical interventions for diabetes mellitus on beta cell metabolism in vivo in the same islets over an extended period of time.

Funding. Larry L. Hillblom Foundation (2014-D-001-NET, 2021-D-007-FEL).

Disclosures. The authors declare no conflicts of interest.

Data availability. Data underlying the results presented in this paper are available in Ref. [23].

Supplemental document. See Supplement 1 for supporting content.

References

1. S. Speier, D. Nyqvist, O. Cabrera, J. Yu, R. D. Molano, A. Pileggi, T. Moede, M. Köhler, J. Wilbertz, B. Leibiger, A. Caicedo, and P. O. Berggren, "Noninvasive in vivo imaging of pancreatic islet cell biology," Nat. Med. **14**(5), 574–578 (2008).
2. S. Speier, D. Nyqvist, M. Köhler, A. Caicedo, I. B. Leibiger, and P. O. Berggren, "Noninvasive high-resolution in vivo imaging of cell biology in the anterior chamber of the mouse eye," Nat. Protoc. **3**(8), 1278–1286 (2008).
3. E. Ilegems, A. Dicker, S. Speier, A. Sharma, A. Bahow, P. K. Edlund, I. B. Leibiger, and P.-O. Berggren, "Reporter islets in the eye reveal the plasticity of the endocrine pancreas," Proc. Natl. Acad. Sci. **110**(51), 20581–20586 (2013).
4. Z. Wang, T. Gurlo, A. V. Matveyenko, D. Elashoff, P. Wang, M. Rosenberger, J. A. Junge, R. C. Stevens, K. L. White, and S. E. Fraser, "Live-cell imaging of glucose-induced metabolic coupling of β and α cell metabolism in health and type 2 diabetes," Commun. Biol. **4**(1), 594 (2021).
5. J. R. Lakowicz, H. Szmacinski, K. Nowaczyk, and M. L. Johnson, "Fluorescence lifetime imaging of free and protein-bound NADH," Proc. Natl. Acad. Sci. **89**(4), 1271–1275 (1992).
6. C. Berclaz, D. Szlag, D. Nguyen, J. Extermann, A. Bouwens, P. J. Marchand, J. Nilsson, A. Schmidt-Christensen, D. Holmberg, A. Grapin-Botton, and T. Lasser, "Label-free fast 3D coherent imaging reveals pancreatic islet micro-vascularization and dynamic blood flow," Biomed. Opt. Express **7**(11), 4569–4580 (2016).
7. M. H. Abdulreda, R. D. Molano, G. Faleo, M. Lopez-Cabezas, A. Shishido, U. Ulissi, C. Fotino, L. F. Hernandez, A. Tschiggfrie, V. R. Aldrich, A. Tamayo-Garcia, A. S. Bayer, C. Ricordi, A. Caicedo, P. Buchwald, A. Pileggi, and P. O. Berggren, "In vivo imaging of type 1 diabetes immunopathology using eye-transplanted islets in NOD mice," Diabetologia **62**(7), 1237–1250 (2019).
8. G. Li, B. Wu, M. G. Ward, A. C. Chong, S. Mukherjee, S. Chen, and M. Hao, "Multifunctional in vivo imaging of pancreatic islets during diabetes development," J. Cell Sci. **129**(14), 2865–2875 (2016).
9. V. Salem, L. D. Silva, and K. Suba, *et al.*, "Leader β-cells coordinate Ca(2+) dynamics across pancreatic islets in vivo," Nat. Metab. **1**(6), 615–629 (2019).
10. J. F. Rivera, S. Costes, T. Gurlo, C. G. Glabe, and P. C. Butler, "Autophagy defends pancreatic β cells from human islet amyloid polypeptide-induced toxicity," J. Clin. Invest. **124**(8), 3489–3500 (2014).
11. C. J. Zuurbier, A. Koeman, S. M. Houten, M. W. Hollmann, and W. J. Florijn, "Optimizing anesthetic regimen for surgery in mice through minimization of hemodynamic, metabolic, and inflammatory perturbations," Exp. Biol. Med. **239**(6), 737–746 (2014).

Biomedical Optics EXPRESS

12. M. F. Chan and Z. Werb, "Confocal imaging of myeloid cells in the corneal stroma of live mice," Bio. Protoc. **5**(13), e1517 (2015).
13. J. R. Lakowicz, *Principles of Fluorescence Spectroscopy* (Springer, 2006).
14. G. Krishnamoorthy, N. Periasamy, and B. Venkataraman, "On the origin of heterogeneity of fluorescence decay kinetics of reduced nicotinamide adenine dinucleotide," Biochem. Biophys. Res. Commun. **144**(1), 387–392 (1987).
15. M. C. Skala, K. M. Riching, D. K. Bird, A. Gendron-Fitzpatrick, J. Eickhoff, K. W. Eliceiri, P. J. Keely, and N. Ramanujam, "In vivo multiphoton fluorescence lifetime imaging of protein-bound and free nicotinamide adenine dinucleotide in normal and precancerous epithelia," J. Biomed. Opt. **12**(2), 024014 (2007).
16. T. S. Blacker, Z. F. Mann, J. E. Gale, M. Ziegler, A. J. Bain, G. Szabadkai, and M. R. Duchen, "Separating NADH and NADPH fluorescence in live cells and tissues using FLIM," Nat. Commun. **5**(1), 3936 (2014).
17. R. Leben, M. Köhler, H. Radbruch, A. E. Hauser, and R. A. Niesner, "Systematic enzyme mapping of cellular metabolism by phasor-analyzed label-free NAD(P)H fluorescence lifetime imaging," Int. J. Mol. Sci. **20**(22), 5565 (2019).
18. S. Rodimova, D. Kuznetsova, N. Bobrov, V. Elagin, V. Shcheslavskiy, V. Zagainov, and E. Zagaynova, "Mapping metabolism of liver tissue using two-photon FLIM," Biomed. Opt. Express **11**(8), 4458–4470 (2020).
19. T. K. Bratanova-Tochkova, H. Cheng, S. Daniel, S. Gunawardana, Y.-J. Liu, J. Mulvaney-Musa, T. Schermerhorn, S. G. Straub, H. Yajima, and G. W. G. Sharp, "Triggering and augmentation mechanisms, granule pools, and biphasic insulin secretion," Diabetes **51**(suppl_1), S83–S90 (2002).
20. A. A. Christensen and M. Gannon, "The Beta Cell in Type 2 Diabetes," Curr. Diab. Rep. **19**(9), 81 (2019).
21. C. Montemurro, H. Nomoto, L. Pei, V. S. Parekh, K. E. Vongbunyong, S. Vadrevu, T. Gurlo, A. E. Butler, R. Subramaniam, E. Ritou, O.S. Shirihai, L. S. Satin, P. C. Butler, and S. Tudzarova, "IAPP toxicity activates HIF1α/PFKFB3 signaling delaying β-cell loss at the expense of β-cell function," Nat. Commun. **10**(1), 2679 (2019).
22. H. Nomoto, L. Pei, C. Montemurro, M. Rosenberger, A. Furterer, G. Coppola, B. Nadel, M. Pellegrini, T. Gurlo, P. C. Butler, and S. Tudzarova, "Activation of the HIF1α/PFKFB3 stress response pathway in beta cells in type 1 diabetes," Diabetologia **63**(1), 149–161 (2020).
23. T. Gurlo, "FLIM," Open Science Framework, 2023, https://osf.io/8ef54/?view_only=85b38968486145f1a1e06857db2c3295.